NANO LETTERS

pubs.acs.org/NanoLett

Modulating the Electronic Properties along Carbon Nanotubes via Tube–Substrate Interaction

Jaqueline S. Soares,[†] Ana Paula M. Barboza,[†] Paulo T. Araujo,[†] Newton M. Barbosa Neto,[†,‡] Denise Nakabayashi,[†] Nitzan Shadmi,[§] Tohar S. Yarden,[§] Ariel Ismach,[§] Noam Geblinger,[§] Ernesto Joselevich,[§] Cecilia Vilani,[∥] Luiz G. Cançado,[†,⊥] Lukas Novotny,[⊥] Gene Dresselhaus,[#] Mildred S. Dresselhaus,[▽] Bernardo R. A. Neves,[†] Mario S. C. Mazzoni,[†] and Ado Jorio*[,†]

[†]Departamento de Física, Universidade Federal de Minas Gerais, Belo Horizonte, MG, 31270-901, Brazil, [‡]Instituto de Física, Universidade Federal de Uberlândia, Uberlândia, MG, 38400-902, Brazil, [§]Department of Materials and Interfaces, Weizmann Institute of Science, Rehovot, 76100, Israel, [∥]Divisão de Metrologia de Materiais, Instituto Nacional de Metrologia, Normalização e Qualidade Industrial (INMETRO), Duque de Caxias, RJ, 25250-020, Brazil, [⊥]Institute of Optics, University of Rochester, Rochester, New York 14627, United States, [#]Francis Bitter Magnet Laboratory, Massachusetts Institute of Technology, Cambridge, Massachusetts 02139, United States, and [▽]Department of Physics and Department of Electrical Engineering and Computer Science, Massachusetts Institute of Technology, Cambridge, Massachusetts 02139, United States

ABSTRACT We study single wall carbon nanotubes (SWNTs) deposited on quartz. Their Raman spectrum depends on the tube–substrate morphology, and in some cases, it shows that the same SWNT-on-quartz system exhibits a mixture of semiconductor and metal behavior, depending on the orientation between the tube and the substrate. We also address the problem using electric force microscopy and ab initio calculations, both showing that the electronic properties along a single SWNT are being modulated via tube–substrate interaction.

KEYWORDS Carbon nanotubes, tube–substrate interaction, Raman spectroscopy, electric force microscopy, quartz

Single wall carbon nanotubes (SWNTs) are quasi-one-dimensional structures consisting of a rolled up graphene nanoribbon.[1−4] Due to their unusually large surface-to-volume ratio, SWNTs are strongly affected by the environment.[5] Contact with a supporting substrate modifies their properties, and such interactions have been broadly studied as either a drawback or a solution for developing nanotube-based nanotechnologies.[6−23] Researchers have for example studied the interaction of SWNTs with silicon substrates[6,8,10,13−16,19] as a possible route for the integration between SWNTs and silicon-based microelectronics. Ab initio calculations for small diameter SWNTs adsorbed on unpassivated Si surfaces predict stable structures through the formation of covalent Si–C bonds.[8,13−15] Other substrates have also been studied,[11,17,20−22] with quartz becoming identified as a promising substrate for the epitaxial growth of SWNTs.[17,20−22] With the development of nanotube epitaxy combined with the controlled application of external forces, which can generate complex carbon nanotube structures,[17,20−22] the effect of nanotube–substrate interaction can be controlled and measured along the same physical nanotube, as reported here.

Carbon nanotubes were grown by catalytic chemical vapor deposition (CVD) on miscut single-crystal quartz wafers, as previously reported.[17] The resulting vicinal α-SiO_2 $(1\bar{1}01)$ substrate is insulating, and terminated with parallel atomic steps.[17] At the temperature of nanotube growth, the surface contains exposed unpassivated Si atoms,[24] thus promoting a strong tube–substrate interaction, especially when the nanotube lies *along* a step.[8,13−15] Alternatively, when the nanotube lies *across* the surface steps, the interaction is discontinuous and weaker. Nanotube epitaxy combined with gas flow directed growth[17,20−22] leads to the formation of carbon nanotube *serpentines* (see Figure 1a,b), i.e., SWNTs with parallel straight segments (labeled S_1, S_2, S_3, ..., in Figure 1b) connected by alternating U-turns (labeled U_{12}, U_{23}, U_{34}, ..., in Figure 1b). The straight segments usually lie *along* the quartz steps, while the U-turns lie *across* the steps (see Figure 1b), so that the tube–substrate interaction is modulated along the tube.

The main physical effects that have to be revealed and studied in this tube–substrate system are strain and charge transfer and how these effects vary when changing the orientation between the nanotube and the quartz surface steps. Strain depends not only on the tube–substrate interaction but also on the dynamics of the serpentine formation process, which involves a competition between the tube–

* To whom correspondence should be addressed, adojorio@fisica.ufmg.br.
Received for review: 09/14/2010
Published on Web: 11/04/2010

DOI: 10.1021/nl103245q | *Nano Lett.* **2010,** *10,* 5043–5048

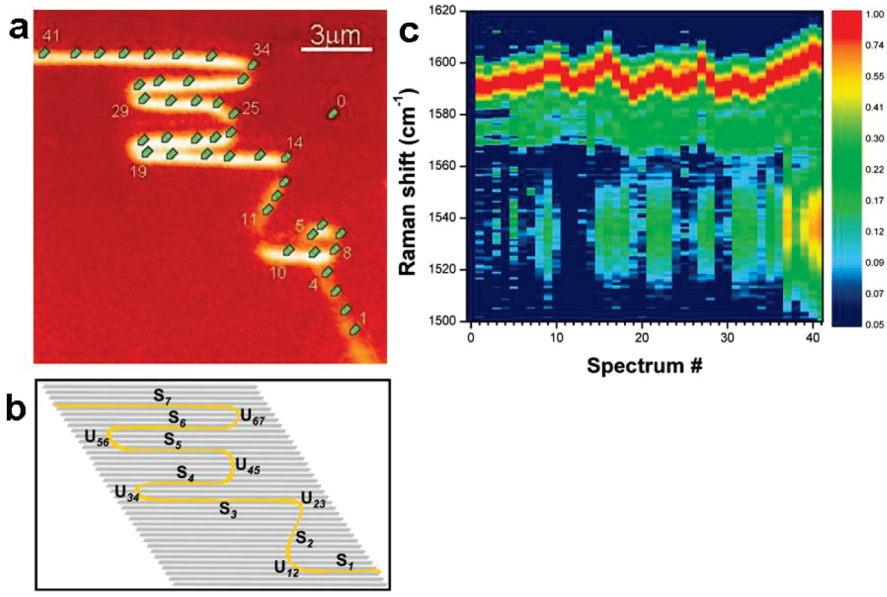

FIGURE 1. Raman spectra along a SWNT serpentine on (1$\bar{1}$01) quartz. (a) Confocal image of the G-band integrated intensity (E_{laser} = 1.96 eV, spatial resolution ~500 nm). The spectral intensity is stronger in segments aligned along the steps because of the light polarization dependence for Raman scattering (the light was polarized along the tube axis).[25] Changing the light polarization with respect to the sample changes the overall intensities but does not change the Raman lineshapes. (b) Schematics of part of the SWNT serpentine in (a) (yellow) on top of the miscut quartz. Miscut means the quartz was polished with a small angle with respect to the atomic layers, so that the substrate exhibits atomic steps (gray lines). The straight segments are labeled by S_i, with i = 1, 2, 3, ..., numbering the segments according to the growth direction (from point 1 to 41 in (a) (see Supporting Information)). The U-turns are labeled by U_{jk}, which are the U-turns connecting segments S_j and S_k. (c) The G-band Raman spectra obtained at the 41 points indicated by vertical green pointers and numbered in (a). There is a blue shift and red shift of the higher frequency G^+ feature (~1590−1605 cm^{-1}) along with the appearance and disappearance of the lower frequency G^- feature (~1540 cm^{-1}), related to the tube−substrate morphology and interaction.

surface interaction and the gas-flow-related drag forces.[17] Raman spectroscopy is the ideal tool for analyzing the tube−substrate interaction without disturbing the tube−surface interaction.[25] Analysis of the tangential stretching mode frequency and line shape (named the G band, at 1500−1600 cm^{-1}, see Figure 1c)[25] can be used to measure strain[26−28] and doping[29−31] and to distinguish between metallic and semiconducting tubes,[25] because of the presence of a Kohn anomaly in the phonon dispersion of metallic SWNTs.[30−32] In addition, frequency shifts of the dominant second-order mode (G′ band, at 2600−2700 cm^{-1}) can also be used to differentiate between electron donor (n) and acceptor (p) doping, even at the individual single atom doping level.[33] These aspects of Raman spectroscopy are exemplified in the three representative Raman spectra shown in Figure 2. Spectra (a) and (b) were taken at different locations of the same nanotube, whereas spectrum (c) was taken on a different nanotube. The G-band features in spectrum (a) are typical of a semiconducting SWNT, with two sharp Lorentzian peaks,[25] G^+ and G^-. The G-band features in spectrum (c) are typical of a metallic nanotube,[25] with a large downshift and broadening of the G^- peak. The G band features in spectrum (b) show a superposition of metal and semiconducting behavior. Spectra (a) and (c) both show a G′ band with a single peak, while spectrum (b) shows a splitting of the G′ band. According to ref 33, the shifts in the G′ band features between spectra (a) and (c) can be explained by doping, which can cause either an upshift or

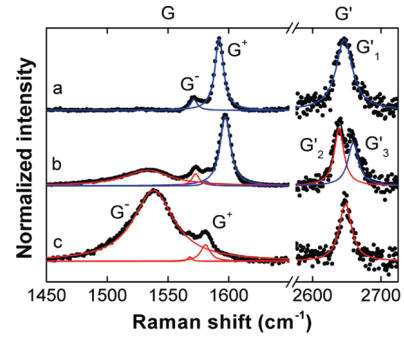

FIGURE 2. Spectroscopic analysis of two SWNT serpentines grown on quartz. (a) and (b) come from the same serpentine in Figure 1a, differing with regard to the tube orientation with respect to the substrate, i.e., *across* (S_2 in Figure 1b) vs *along* (S_3 in Figure 1b) the surface steps, respectively. Spectrum (a) exhibits a G band with a line shape typical of a semiconducting SWNT. Spectrum (b) exhibits a G band with a line shape showing a mixture of lineshapes typical of semiconducting (blue Lorentzians) and a metallic (red Lorentzians) SWNT behavior. Note that the G′ peak splits in (b). (c) The G and G′ bands of a different serpentine SWNT exhibiting a G band with a metallic character, irrespective of tube orientation with regard to the substrate steps.

downshift due to doping, with respect to spectra (a) and (c). The surprise is that the spectra (a) and (b) were measured from one single SWNT serpentine on quartz, the one shown in Figure 1. The difference between (a) and (b) in Figure 2 is that, in (b) the tube lies *along* the surface steps, while in (a) the tube lies *across* the steps.

DOI: 10.1021/nl103245q | *Nano Lett.* **2010,** *10,* 5043−5048

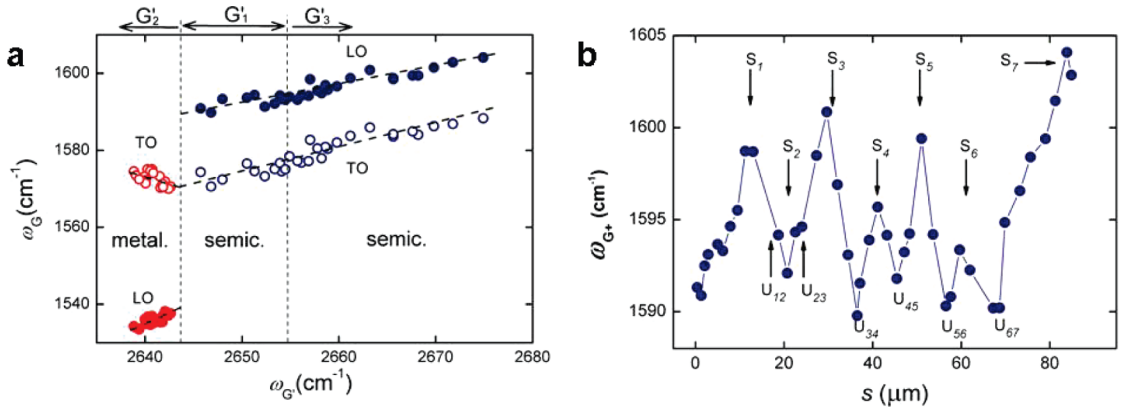

FIGURE 3. Strain and doping effects on the SWNT G and G′ Raman bands. (a) Relation between ω_G and $\omega_{G'}$ for the SWNT serpentine shown in Figures 1 and 2a,b. When the tube is making the U-turn, the G′ band exhibits a single peak, named G′$_1$, while the G band exhibits two peaks, characteristic of a semiconducting SWNT. When the tube is aligned along a substrate step, the G′ band exhibits two peaks, named G′$_2$ and G′$_3$, while the G band exhibits four peaks, two characteristic of a semiconducting SWNT (blue symbols) and two characteristic of a metallic SWNT (red symbols). Not all the 41 G band data sets from Figure 1 are shown here because the G′ band is absent in 12 cases. (b) The G$^+$ frequency of semiconducting SWNTs (LO mode) observed at the 41 points shown in Figure 1a is plotted as a function of the distance *s* from point #1 measured along the SWNT. S$_i$ and U$_{jk}$ locate the center of the straight segments and U-turns, respectively (see Figure 1b), showing that the frequency changes are correlated with the tube−substrate morphology. The frequency uncertainty is better than ±2 cm^{-1}.

To understand the spectral evolution between (a) and (b) in Figure 2, we took spectra at different locations along the same nanotube serpentine of Figure 2a,b, as shown by the 41 locations indicated in Figure 1a. The confocal image shown in Figure 1a was obtained by integrating of the G-band Raman signal from the SWNT serpentine while scanning the sample. Figure 1c shows the G-band spectra obtained from all 41 points indicated by the vertical green pointers in Figure 1a. Analysis of the spectral features shows that the G-band spectra look like the semiconducting profile (a) in Figure 2 when crossing the atomic steps (U-turns and straight lines passing through points 11−14, named S$_2$ in Figure 1b), while at segments parallel to the steps, such as points 15−18 (S$_3$ in Figure 1b), the spectra look like spectrum (b) in Figure 2. There is a variation in the higher frequency G$^+$ feature (∼1590−1605 cm^{-1}), which is also related to the tube−substrate morphology, as discussed below.

Figure 3 shows the frequency behavior for both the G and G′ bands (ω_G vs $\omega_{G'}$) as a method to characterize the strain[26−28] and doping[29−31] induced by the tube−substrate interaction and to understand the observation of a mixed metal−semiconductor behavior such as found in spectrum (b) in Figure 2. As mentioned earlier, the G band in semiconducting SWNTs is composed of two peaks; the higher frequency G$^+$ feature is related to the C−C stretching mode along the tube axis and is named the longitudinal optical (LO) mode, while the lower frequency G$^-$ feature is related to C−C stretching along the tube circumference and is named the transverse optical (TO) mode.[25] Their frequencies (ω) depend sensitively on strain[26−28] and doping,[29−31] and when the tube becomes metallic, the Kohn anomaly appears for the LO phonon, which decreases ω_G^{LO} and broadens the peak.[30,32] In Figure 3a, ω_G^{LO} and ω_G^{TO}, which are observed at the 41 points along the SWNT serpentine depicted in Figure 1, are plotted as a function of the G′ band frequency ($\omega_{G'}$, second-order feature related to a breathing of the carbon hexagons) observed at the same points. Points located at the portions of the serpentine crossing the atomic steps exhibit only one G′ peak, which we call G′$_1$, and two G band peaks characteristics of semiconducting SWNTs (see spectrum (a) in Figure 2 and also the region between the two dashed vertical lines in Figure 3a). Points where the nanotube lies along to the steps exhibit two G′ peaks (see spectrum (b) in Figure 2), which we call G′$_2$ and G′$_3$, respectively, in Figure 3a. At these locations, the G band exhibits four peaks, two of which show a line shape characteristic of a semiconducting SWNT and two of which show a line shape characteristic of a metallic SWNT (blue and red Lorentzians in spectrum (b) of Figure 2, respectively). The two G band peaks characteristic of a semiconducting tube exhibit a smooth correlation between the G′$_1$ frequency and the G′$_3$ frequency (blue symbols in Figure 3a). The higher frequency G peak characteristic of metallic SWNTs (TO) exhibits a frequency that correlates with that of G′$_2$ (red symbols in Figure 3a), while the LO mode frequency is strongly redshifted, as expected due to the Kohn anomaly.[30,32] The behavior shown in Figure 3a suggests that the G′$_2$ peak is related to a metallic SWNT, while the G′$_3$ is related to a semiconducting SWNT. It is known that n (p) doping causes a downshift (upshift) in the G′ frequency[33].

In Figure 3b, the ω_G^{LO} frequency for semiconducting SWNTs is plotted as a function of the distance *s* from point #1, which is measured along the SWNT. Clearly the ω_G^{LO} is observed to oscillate, showing maxima at the center of the straight tube segments (labeled S$_i$ in Figures 3b and 1b) and minima at the center of the U-turns (labeled U$_{jk}$ in Figures 3b and 1b). Larger frequencies indicate stronger strain[26−28] and doping,[29−31] thus corroborating the stronger vs weaker modulated tube−substrate interaction when the nanotube

DOI: 10.1021/nl103245q | *Nano Lett.* **2010,** *10,* 5043−5048

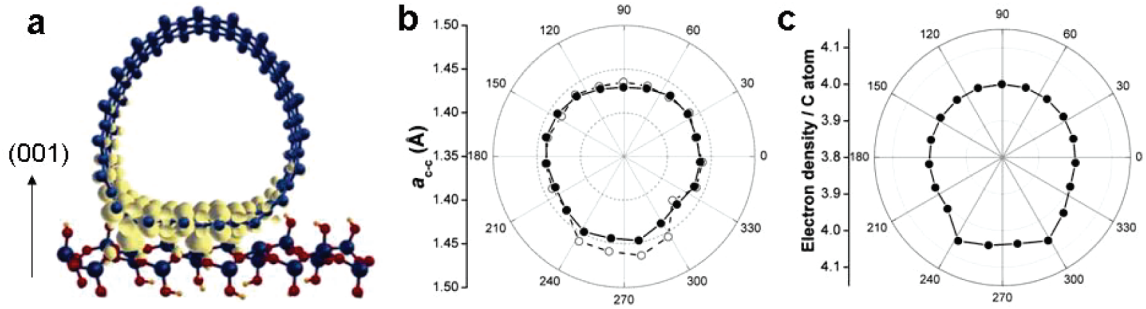

FIGURE 4. Modeling the tube−substrate interaction based on pseudopotential DFT. (a) Real space representation of the electronic states at the Fermi level of the distorted tube. The (19,0) SWNT is sitting on the (001) surface of a SiO_2 substrate (see arrow) with tube axis along (100). (b) Average bond length (a_{C-C}) along the tube axis (open circles) and along the tube circumference (filled circles), and (c) the electron per carbon atom density (ρ) of the SWNT deposited on a quartz substrate. In this polar representation, a_{C-C} and ρ change along the tube circumference, the values varying from the center to the edge of the circle, as quantified by the axis on the left, which applies for 90° and 270°. The a_{C-C} increases at the tube−substrate contact region (240−300°). The electron density and bond lengths change around the circumference, and the changes exhibit maxima near the tube−substrate contact region.

lies along versus across the surface steps. The modulation of ω_G^{LO} along the straight segments, on the other hand, can be attributed to oscillations in the strain along the nanotube resulting from the competition between the tube−surface interaction and the aerodynamic drag forces during the formation of the serpentine, consistent with the "falling spaghetti" mechanism previously proposed.[17] All the maximal ω_G^{LO} values correspond to the center of the straight segments aligned along a quartz step. The fact that the misaligned straight segment S_2 actually shows a minimum in ω_G^{LO} indicates that the effect of tube−surface interaction on the electronic properties of the nanotube is relatively stronger than that of strain, while the remaining effect of the aerodynamic drag forces should be responsible for the smaller ω_G^{LO} maxima for the S_i's with even i. Scanning electron microscopy shows the serpentine growth happened from point 1 to 41, so that i odd indicate straight segments falling to the left, while i even indicate straight segments falling to the right, taking Figure 1a as a reference (check the "falling spaghetti" mechanism[17]). Therefore, the larger ω_G^{LO} maxima for S_i odd indicate that, during the "falling spaghetti" process, there was a gas-flow drag component pointing to the left. This asymmetry can be attributed to the fact that the flow was not perfectly perpendicular to the steps (see Supporting Information). All these effects are stable as a function of the sample lifetime, since this study was carried out within 2 years time after the growth.

To shed light in our findings, we performed first-principles calculations for a nanotube placed on top of a crystalline SiO_2 substrate. Our calculations are based on pseudopotential Density Functional Theory (DFT)[34−36] formalism, as implemented in the SIESTA program,[37,38] which makes use of a basis set composed of pseudo atomic functions of finite range. To fully justify this strong tube−substrate interaction, we developed different models where the SWNTs are in contact with nonpassivated surfaces, with either Si or O exposed (see Supporting Information). One of the modeled systems is shown in Figure 4a after geometry relaxation. We consider in the calculation a (19,0) carbon nanotube sitting on the (001) surface of a SiO_2 substrate. The (19,0) has a diameter of 1.4 nm, matching the diameter of the tube analyzed in Figures 1−3 (see Supporting Information). Upon relaxation, the silicon atoms in the contact region are found to experience an upward displacement and the bottom part of the nanotube becomes flat. The deformation is the result of a strong interaction between carbon bonding states and surface dangling bonds, which show up in the band structure as dispersive bands crossing the Fermi level (see Supporting Information). The yellowish clouds in Figure 4a represent a plot of the electronic density for states within energies of up to 0.1 eV around the Fermi level. Therefore, the bands responsible for the gap closure are predominantly localized spatially in the contact region along the flat surface of the nanotube. These calculations elucidate how a strong nanotube−substrate adhesion of the nanotube along an exposed SiO_2 surface rehybridizes the electronic states to produce two tube segments (bottom and top with respect to the substrate) with different electronic configurations, thus explaining the mixed metal−semiconducting character observed in the Raman spectroscopy measurements (Figures 1−3). Such kind of hybrid structure requires flat crystalline substrates to be present, where the interaction is extended and does not generate localized states.

For a more theoretical quantitative analysis, parts (b) and (c) of Figures 4 show how the substrate affects the bond lengths (strain) and charge distribution (doping) around the tube circumference, respectively. Figure 4b shows that the average distance between carbon atoms (a_{C-C}) increases when the tube is in contact with the substrate, with $\Delta a_{C-C}^{Max} \sim 1.7\%$. A slightly larger increase is observed for the a_{CC} measured along the tube axis (open circles), suggesting a stronger effect should be felt by ω_G^{LO}. Figure 4c shows that the average density of electrons per carbon atom also increases in the tube−substrate contact region, changing from the expected value of 4 electrons/C (the two 1s core electrons are not considered in our model) to up to ~4.05 electrons/C at the surface. Increase in bond lengths should soften the tangential mode frequencies, but this effect is

DOI: 10.1021/nl103245q | *Nano Lett.* **2010,** *10,* 5043--5048

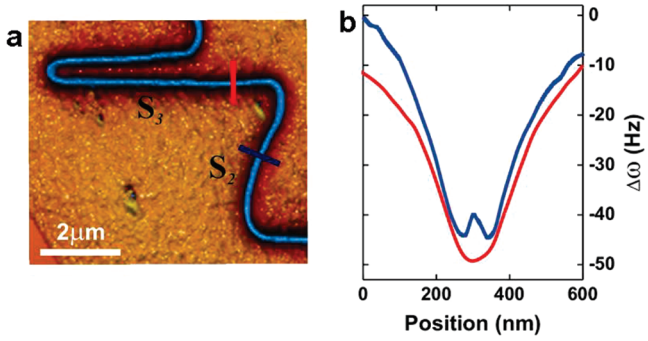

FIGURE 5. Electric force microscopy (EFM) analysis of the alternating metal−semiconductor carbon nanotube heterojunction. (a) EFM image of the same SWNT serpentine discussed in Figure 1 (Experimental conditions: $V = -5$ V; lift height, 50 nm; $\omega_0 = 27.6$ kHz; $k = 0.60$ N/m). (b) Scanning across the SWNT, the cantilever frequency shift is different if a tube is semiconducting ("W-shaped" blue line) or metallic ("V-shaped" red line) (see Supporting Information). The profiles in (b) are as measured. The red and dark blue lines in (a) indicate the two regions where these profiles in (b) were acquired, which correspond to S_3 and S_2 in Figure 1b, respectively.

compensated by the phonon stiffening expected by the disappearance of the Kohn anomaly due to doping. We cannot clearly distinguish in our experiment between the spectral changes arising from strain and those arising from doping, and these effects are probably correlated to achieve structure equilibrium, as indicated by parts (b) and (c) of Figure 4.

Although the results discussed here are based on data from one SWNT, we have studied nine SWNT serpentines, and significant spectral modifications clearly related to the anisotropic tube−substrate interaction could be identified in all of them (see Supporting Information). In all nine cases the frequencies of the G and G′ bands change according to the orientation between the tube axis and the crystalline quartz substrate, consistent with the results shown here. The detailed frequency changes vary from sample to sample indicating a possible (n,m) dependence, where both the tube diameter and the angle between the hexagons and the SiO_2 substrate could play a role. The influence of tube curvature is negligible, since the U-turns are in the order of 1 μm diameter while the tube is 1 nm in diameter. The importance of defects is also excluded by the complete absence of the defect induced D band ($\sim$1350 cm^{-1}) in both far-field and near-field Raman spectroscopy imaging (see Supporting Information). The modulated doping-strain, generating mixed metal−semiconductor Raman profiles have been observed in four different serpentines. When the tube exhibits spectra characteristic of a metallic system (one tube measured), the mixed behavior was not observed. This is supported by our DFT calculations, since metallic tubes always have electrons crossing the Fermi level (see Supporting Information).

For completeness, we have also employed electric force microscopy (EFM) characterization of the SWNT serpentine for the direct determination of its metallicity. Figure 5 shows the EFM analysis of the same SWNT discussed in Figure 1. The nanotube appears in the image as regions of negative frequency shifts (in blue) contrasting with the quartz substrate (in brown). Even though the EFM signal seems homogeneous in Figure 5a, a more careful analysis reveals structure in the line shape, as shown in the line profiles across two different regions in the nanotube presented in Figure 5b. As discussed in ref 39, the different polarizabilities of metallic nanotubes on substrate versus semiconducting nanotubes on substrate create a distinct coupling with the electric field emanating from the EFM tip for each case. These differences result in a "W-shaped" EFM line profile across a semiconducting tube, while a metallic SWNT portrays a "V-shaped" line profile (see Supporting Information for an schematic explaining the effect). The red and blue profiles in Figure 5b correspond to the regions marked by the red and dark blue lines in Figure 5a, respectively. The "W-shaped" dark blue profile, typical for a region with weak substrate interaction, is the EFM signature for a semiconducting nanotube, whereas the "V-shaped" red profile, typical for a strong substrate interaction region, attests to a metallic behavior for this region of the SWNT. Therefore, the EFM results shown in Figure 5 corroborate the metal−semiconducting alternating behavior of our SWNT serpentine Raman spectra.

In summary, we have measured a SWNT−substrate system where the tube substrate interaction can be tuned by changing the tube−substrate orientation. The effects on the electronic and vibrational properties of the SWNTs, observed using resonance Raman spectroscopy and electric force microscopy, indicate important changes in the properties depending on the tube−substrate orientation. These changes are clearly related to the tube−substrate interaction resulting from the tube−substrate morphology and formation dynamics. The periodic change on the tube−substrate interaction existing in our SWNT serpentines seems to generate a set of alternate doped−undoped tube segments, and different complex superlattices could be created through substrate engineering. Interestingly, Huang and Choi[21] observed that the length-normalized resistance of carbon nanotube serpentines increases with the number of U-turns, and such behavior was explained by the presence of defects in the curved regions. Our finding can explain the results observed in ref 21 with perfectly crystalline junctions, where the "defects" would be the substrate changing the tube electronic behavior. This is supported by our Raman spectroscopy results with the complete absence of the disorder-induced D-band peak ($\sim$1300 cm^{-1}), which is normally observed in defective sp^2 carbon materials.[25]

Acknowledgment. A.J., M.S.C.M., and B.R.A.N. acknowledge financial support from Rede Nacional de SPM, Rede Nacional de Pesquisa em Nanotubos de Carbono, Instituto de Nanotecnologia (MCT-CNPq), and AFOSR/SOARD (award #FA9550-08-1-0236). L.N. acknowledges financial support from the U.S. Department of Energy (Grant DE-FG02-05ER46207). E.J. acknowledges support from the Israel Science Foundation, the US−Israel Binational Science Foun-

DOI: 10.1021/nl103245q | *Nano Lett.* **2010,** *10,* 5043–5048

dation, the Kimmel Center for Nanoscale Science, and the Legrain, Djanogly, Alhadeff, and Perlman Family foundations. M.S.D. acknowledges NSF DMR # 07-04197.

Supporting Information Available. This material is available free of charge via the Internet at http://pubs.acs.org.

REFERENCES AND NOTES

(1) Iijima, S.; Ichihashi, T. *Nature* **1993**, *363*, 603–605.
(2) Yu, D.; Liu, F. *Nano Lett.* **2007**, *7*, 3046–3050.
(3) Jiao, L.; Zhang, L.; Wang, X.; Diankov, G.; Dai, H. *Nature* **2009**, *458*, 877–880.
(4) Santos, H.; Chico, L.; Brey, L. *Phys. Rev. Lett.* **2009**, *103*, 086801.
(5) Jorio, A.; Dresselhaus, M. S. *MRS Bull.* **2007**, *32*, 988–993.
(6) Heertel, T.; Walkup, R. E.; Avouris, Ph. *Phys. Rev. B* **1998**, *58*, 13870–13873.
(7) Mazzoni, M. S. C.; Chacham, H. *Appl. Phys. Lett.* **2000**, *76*, 1561–1563.
(8) Orellana, W.; Miwa, R. H.; Fazzio, A. *Phys. Rev. Lett.* **2003**, *91*, 166802.
(9) Jiang, C.; Zhao, J.; Therese, H. A.; Friedrich, M.; Mews, A. *J. Phys. Chem. B* **2003**, *107*, 8742–8745.
(10) Tsukruk, V. V.; Ko, H.; Peleshanko, S. *Phys. Rev. Lett.* **2004**, *92*, 065502.
(11) Kim, Y.-H.; Heben, M. J.; Zhang, S. B. *Phys. Rev. Lett.* **2004**, *92*, 176102.
(12) Ismach, A.; Segev, L.; Wachtel, E.; Joselevich, E. *Angew. Chem., Int. Ed* **2004**, *43*, 6140–6143.
(13) Miwa, R. H.; Orellana, W.; Fazzio, A. *Appl. Phys. Lett.* **2005**, *86*, 213111.
(14) Berber, S.; Oshiyama, A. *Phys. Rev. Lett.* **2006**, *96*, 105505.
(15) Peng, G. W.; Huan, A. C. H.; Liu, L.; Feng, Y. P. *Phys. Rev. B* **2006**, *74*, 235416.
(16) Albrecht, P. M.; Lyding, J. W. *Nanotechnology* **2007**, *18*, 125302.
(17) Geblinger, N.; Ismach, A.; Joselevich, E. *Nat. Nanotechnol.* **2008**, *3*, 195–200.
(18) Barboza, A. P. M.; Gomes, A. P.; Archanjo, B. S.; Araújo, P. T.; Jorio, A.; Ferlauto, A. S.; Mazzoni, M. S. C.; Chacham, H.; Neves, B. R. A. *Phys. Rev. Lett.* **2008**, *100*, 256804.
(19) You, Y.; Yu, T.; Kasim, J.; Song, H.; Fan, X.; Ni, Z.; Cao, L.; Jiang, H.; Shen, D.; Kuo, J.; Shen, Z. *Appl. Phys. Lett.* **2008**, *93*, 103111.
(20) Jeon, S.; Lee, C.; Tang, J.; Hone, J.; Nuckolis, C. *Nano Res.* **2008**, *1*, 427–433.
(21) Huang, J.; Choi, W. *Nanotechnology* **2008**, *19*, 505601.
(22) Xiao, J.; Dunham, S.; Liu, P.; Zhang, Y.; Kocabas, C.; Moh, L.; Huang, Y.; Hwang, K.-C.; Lu, C.; Huang, W.; Rogers, J. A. *Nano Lett.* **2009**, *9*, 4311–4319.
(23) Steiner, M.; Freitag, M.; Tsang, J. C.; Perebeinos, V.; Bol, A. A.; Failla, A. V.; Avouris, Ph. *Appl. Phys. A* **2009**, *96*, 271–282.
(24) Viefhaus, H.; Rossow, W. *Surf. Sci.* **1984**, *141*, 341–354.
(25) Dresselhaus, M. S.; Dresselhaus, G.; Saito, R.; Jorio, A. *Phys. Rep.* **2005**, *409*, 47–99.
(26) Cronin, S. B.; Swan, A. K.; Ünlü, M. S.; Goldberg, B. B.; Dresselhaus, M. S.; Tinkhan, M. *Phys. Rev. Lett.* **2004**, *93*, 167401.
(27) Duan, X.; Son, H.; Gao, B.; Zhang, J.; Wu, T.; Samsonidze, Ge. G.; Dresselhaus, M. S.; Liu, Z.; Kong, J. *Nano Lett.* **2007**, *7*, 2116–2121.
(28) Gao, B.; Jiang, L.; Ling, X.; Zhang, J.; Liu, Z. *J. Phys. Chem. C* **2008**, *112*, 20123–20125.
(29) Das, A.; Sood, A. K.; Govindaraj, A.; Marco Saitta, A.; Lazzeri, M.; Mauri, F.; Rao, C. N. R.; Liu, Z.; Kong, J. *Phys. Rev. Lett.* **2007**, *99*, 136803.
(30) Dubay, O.; Kresse, G.; Kuzmany, H. *Phys. Rev. Lett.* **2002**, *88*, 235506.
(31) Tsang, J. C.; Freitag, M.; Perebeinos, V.; Liu, J.; Avouris, Ph. *Nat. Nanotechnol.* **2007**, *2*, 725–730.
(32) Piscanec, S.; Lazzeri, M.; Robertson, J.; Ferrari, A. C.; Mauri, F. *Phys. Rev. B* **2007**, *75*, 035427.
(33) Maciel, I. O.; Anderson, N.; Pimenta, M. A.; Hartschuh, A.; Qian, H.; Terrones, M.; Terrones, H.; Campos-Delgado, J.; Rao, A.; Novotny, L.; Jorio, A. *Nat. Mater.* **2008**, *7*, 878–883.
(34) Kohn, W.; Sham, L. J. *Phys. Rev.* **1965**, *140*, A1133–A1138.
(35) Kleinman, L.; Bylander, D. M. *Phys Rev. Lett.* **1982**, *48*, 1425–1428.
(36) Troullier, N.; Martins, J. L. *Phys. Rev. B* **1991**, *43*, 1993–1996.
(37) Ordejón, P.; Artacho, E.; Soler, J. M. *Phys. rev. B* **1996**, *53*, R10441–R10444.
(38) Soler, J. M.; Artacho, E.; Gale, J. D.; Garcia, A.; Junquera, J.; Ordejón, P.; Sánchez-Portal, D. J. *Phys.: Condens. Matter* **2002**, *14*, 2745–2779.
(39) Barboza, A. P. M.; Gomes, A. P.; Chacham, H.; Neves, B. R. A. *Carbon* **2010**, *48*, 3287–3292.

DOI: 10.1021/nl103245q | *Nano Lett.* **2010,** *10,* 5043–5048